

# EAST: Environment Aware Safe Tracking using Planning and Control Co-Design

Journal Title  
XX(X):1–16  
©The Author(s) 2023  
Reprints and permission:  
sagepub.co.uk/journalsPermissions.nav  
DOI: 10.1177/ToBeAssigned  
www.sagepub.com/

SAGE

Zhichao Li, Yinzhuang Yi, Zhuolin Niu, Nikolay Atanasov

## Abstract

This paper considers the problem of autonomous robot navigation in unknown environments with moving obstacles. We propose a new method that systematically puts planning, motion prediction and safety metric design together to achieve environmental adaptive and safe navigation. This algorithm balances optimality in travel distance and safety with respect to passing clearance. Robot adapts progress speed adaptively according to the sensed environment, being fast in wide open areas and slow down in narrow passages and taking necessary maneuvers to avoid dangerous incoming obstacles. In our method, directional distance measure, conic-shape motion prediction and custom costmap are integrated properly to evaluate system risk accurately with respect to local geometry of surrounding environments. Using such risk estimation, reference governor technique and control barrier function are worked together to enable adaptive and safe path tracking in dynamical environments. We validate our algorithm extensively both in simulation and challenging real-world environments.

## Keywords

autonomous navigation, safe control, motion planning

## 1 Introduction

In recent years, there has been a rapid emergence of robot applications, thanks to advancements in sensing technology and computation power. These applications are becoming increasingly integrated into human society, such as autonomous driving cars, factory inspection, cleaning services, and medical robotics. Reliable robot navigation is a crucial aspect for enabling these services. As a result, there is a growing focus on researching and developing certifiably safe yet efficient navigation algorithms.

Although there are extensive works on classical motion planning that find optimal paths connecting two states in working space or configuration space. Only a few of them prioritize safety in optimality and system dynamics is often ignored or greatly simplified. In algorithms like ARA\* (Likhachev et al. 2004), RRT\* (Karaman and Frazzoli 2011), optimality usually is often measured in terms of travel distance neglecting robot dynamics. Path clearance is often set to a constant (bigger than robot circumscribed radius). If this constant is small, the resulting optimal paths usually hug tightly to obstacle boundaries and cause downstream tracking controllers vulnerable to collision risk (due to model uncertainty and external disturbances). And a large constant will cause a planner to return no path to areas only connected through narrow

passages. On the other extreme, maximum clearance (Bhattacharya and Gavrilova 2008) can provide the most safe path, however, a much larger travel distance may not be favorable for economic reasons. Ideally, we want a planner that can balance optimality (travel distance) and safety (path clearance) that reach most feasible regions without being super close to obstacles.

In tracking controller design, the performance is usually measured in terms of tracking error and speed. Such design works reasonably well for machines that operate in known, controlled and static environments, like robot arm in manufacturer, airplane on the fly. But, there are many robots applications (for example, floor cleaning robot or autonomous cars) have to work in safe-critical and highly constrained dynamical environments. For these applications, solely using tracking error and speed as objective becomes insufficient and less-favorable. In nature, a intelligent agent tends to control its motion speed

Department of Electrical and Computer Engineering, University of California San Diego, La Jolla, CA 92093.

### Corresponding author:

Zhichao Li, Department of Electrical and Computer Engineering, University of California San Diego, La Jolla, CA 92093.  
Email: zhichaoli@ucsd.edu

according to sensory data. For example, a cat can go through a narrow tunnel or passage cautiously while running fast in wide open area. An experienced driver will pay most attention to objects in front and adjust safe distance properly according to speed, meanwhile being alert to lateral cars but not overly-reacting. From these observations, we see that a good tracking control policy must can estimate risk quickly in real-time and adjust its motion speed adapt to local environments. Plus, while pursuing along the given path, it must be flexible to take necessary detour to reduce collision risk imposed by moving objects. We would like to robot being aware to surrounding environments and can run sufficiently fast when possible in wide-open area and slow down in highly constrained spaces. Furthermore, it needs to pay attention to nearby moving obstacles and able to avoid potential collision and resume to original task quickly.

To address above issues, we develop an environment aware and safe tracking by integrating planning and control design. First, we design a generic customizable cost function connecting planning states and integrated in  $A^*$  planning algorithm. By using distance-based costmap, the planner generate natural (human-like) path balancing safety and clearance, favoring custom clearance in wide open space while being able to go through tight passage. Next, by adopting accurate motion prediction and directional metric, we estimate system running risk with respect to locally sensed environments. Using this estimation, we develop new adaptive reference-governor to track optimized path. It regulates robot motion speed and continuously generate proper signal for low level controller, fast in empty space and slow down when go through places while being reasonable fast in narrow passage. Finally, to handle moving obstacles, we use control barrier functions (CBF) to optimized reference signal (allowing it being away from given path) in minimally invasive fashion. Following this optimized goal, robot can be alert to incoming obstacle and take necessary detours maneuver. When gaining enough safety, robot can resume to original path quickly.

**Contributions.** The two main contributions are summarized as follows. First, on planning side, a new generic cost function is designed and applied to  $A^*$  planner so its output path can balance safety and travel distance. Second on controller design, a new adaptive reference governor is developed using environment aware safety estimation by jointly considering accurate motion prediction and new directional metric. In addition, a novel active governor control policy backed up by CBF function is used to handle moving obstacles. These two aspects are tightly integrated in our design. Our algorithm can navigate the robot fast and safely in complex unknown environments yet being alert to unexpected danger and take necessary action to avoid them. Finally, we validate our algorithm extensively in various

simulated environments, challenging large-scale cluttered unknown office-like indoor collaborative space and outdoor environments with moving obstacles. The code is open source at [here](#).

## 2 Related Works

### 2.1 Graph Search Algorithms

The problem of finding a feasible or optimal path (trajectory) connecting start and goal points (states) has been investigated extensively (LaValle 2006). Sampling-based methods like Probabilistic Roadmap (PRM) (Kavraki et al. 1998), Rapidly-exploring Random Tree (RRT) (LaValle 1998) can quickly find a feasible path even in large scale or high-dimensional space. Some algorithm like RRT\* (Karaman and Frazzoli 2011) can asymptotically converge to the optimal solution. But the non-deterministic property due to sampling procedure and unpredictable intermediate result makes its usage limited especially when application has fixed planning time requirements. Search-based motion planning algorithms like  $A^*$  (Hart et al. 1968) or jump point search (JPS) (Harabor and Grastien 2011) can provide optimal path in a more consistent manner and planning time is predictable. However, search-based algorithms can face scalability issues in large-scale workspace or high-dimensional complex configuration space. If a hard planning time constraints exists, algorithms like ARA\* (Likhachev et al. 2004) and RTAA (Koenig and Likhachev 2006) can be used. In most graph search algorithms, optimality is often equivalent to path length measured in workspace (for mobile robots) and safety is either ignored or simply considered in terms of fixed path clearance. To help further discussion, this type of graph search motion planning algorithm will be referred to geometric planner.

### 2.2 Safety Aware Motion Planning and Trajectory Tracking

For safe-critical robotic applications, system dynamics must be incorporated into motion planning or trajectory tracking. Some researchers bring control theory into planning algorithm design. For example, (Perez et al. 2012) use linear-quadratic-regulation (LQR) cost in steering function design and optimal control is used in (Webb and van den Berg 2013) to connecting sampling states. However, as pointed out by (Pacelli et al. 2018), locally optimal control, does not necessarily lead to global optimality. Moreover, these methods often use simplified system dynamics to reduce computation requirement. The potential tracking error due to model discrepancy can lead to unsafe behavior.

Hierarchical methods using geometric planner as front end followed by trajectory optimization and control techniques as back end also gain lots of attentions. In

(Liu et al. 2017; Gao et al. 2018), a safe flight corridor (a connected safe region in free space) is first constructed for coarse planning task, then trajectory optimization and safe control techniques like model predictive control (MPC) (Gao et al. 2014; Santillo and Jankovic 2020; Bravo et al. 2006) and control barrier function (CBF) (Ames et al. 2019; Borrmann et al. 2015; Ames et al. 2017; Squires et al. 2018) are used. However, such methods require intense online computation resources for flight corridor construction and may not be suitable in complex unknown environments. In many such approaches, we must use simplified dynamics (fully-actuated linear system or differential flat (Fliess et al. 1995)) to ease downstream trajectory optimization and controller design, which limit its usage. To handle general nonlinear dynamics, researchers bring numerical tools for reachable set prediction (Khalil 2002) and use it in safe tracking task. For example, FaSTrack (Herbert et al. 2017) uses Hamilton–Jacobi (HJ) reachability analysis tool (Fisac et al. 2015) to estimate tracking error bounds and develops a safe motion planning algorithm. To mitigate computation burden, the reachability set is pre-computed offline by setting up a pursuit-evasion game between planner and robot dynamics. This setup may lead to unnecessary conservative because planner is considered as adversarial player rather than a cooperative one. Similarly, (Kousik et al. 2020) uses sum-of-square optimization (Papachristodoulou and Prajna 2002) for forward reachable set offline computation and use it to select safe trajectory online.

### 2.3 Environmental Adaptive Motion Control and Planning

In the motion planning algorithm mentioned above, safety is considered as hard constraints. In safe tracking and planning works mentioned above, only system dynamics are considered (in motion prediction). To achieve navigation behavior like smart agents, one needs to develop environmental aware safety metric and integrate in planner and control design.

As mentioned in introduction, a good risk metric should jointly consider system motion and surrounding environment. The author of (Arslan and Koditschek 2017) constructs a dynamic safety metric (DSM) (Garone and Nicotra 2016) using the difference of distance to obstacle and Lyapunov function. Using this DSM, a navigation algorithm is developed using reference-governor techniques for a second order fully-actuated system. In (Li et al. 2020), the author develops a reference-governor path tracker using time-varying ellipsoid motion predictions instead of using Lyapunov function induced invariant set. By embedding directional preference and aligning it with given geometric path using state-dependent directional metric (SDDM), the tracker pays less attention to lateral obstacles

and achieves better performance in corridor-like narrow passages. However, due to front-back symmetry, ellipsoid shape trajectory bound prevents robot gaining speed when leaving obstacle-dense area. To overcome this, EVA-planner (Quan et al. 2021) proposes environmental adaptive safety aware (EASA) by evaluating angle difference using inner product of gradient of Euclidean signed distance field (ESDF) and robot motion direction. However, the volume of free space is neglected which might result in path with insufficient clearance (Liu et al. 2023). In this paper, we use the distance between an accurate cone shape motion prediction (İşleyen et al. 2022) and inflated obstacle space in costmap to serve as our DSM in governor design. Furthermore, by comparing directional DSM and regular, we construct a SDDM-base gain to speed up robot longitudinal motion. The resulting tracker can go fast in narrow passages and quickly speed up when leaving obstacle dense area.

## 3 Problem Formulation

Consider a differential drive ground wheeled robot operating in an unknown environment  $\mathcal{W} \subset \mathbb{R}^2$ . Denote the obstacle space by a closed set  $\mathcal{O}$  and the free space by an open set  $\mathcal{F} := \mathcal{W} \setminus \mathcal{O}$ . The state of the robot  $\mathbf{x}$  consists of its position  $\mathbf{p} = (x, y)$ , orientation  $\theta$ , while its input is the linear speed  $v$  and the steering angular velocity  $\omega$ . Assuming there is no wheel slip, the kinematic model (De Luca et al. 1998) describing the robot’s motion is:

$$\begin{bmatrix} \dot{x} \\ \dot{y} \\ \dot{\theta} \end{bmatrix} = \begin{bmatrix} \cos \theta \\ \sin \theta \\ 0 \end{bmatrix} v + \begin{bmatrix} 0 \\ 0 \\ 1 \end{bmatrix} \omega \quad (1)$$

**Definition 1.** A *path* is a piecewise-continuous function  $\mathcal{P} : [0, 1] \mapsto \text{Int}(\mathcal{F})$  that maps a path-length parameter  $\sigma \in [0, 1]$  to the interior of free space. The start  $\mathcal{P}(0)$  and the end  $\mathcal{P}(1)$  of a navigation path  $\mathcal{P}(\sigma)$  are in the interior of free space, i.e.,  $\mathcal{P}(0), \mathcal{P}(1) \in \text{Int}(\mathcal{F})$ .

**Problem 1.** Given an unknown environment with potential moving obstacles in present, design an environment aware and safe tracking algorithm that drives a differential-drive robot from start to goal locations following paths generated online while exploring the environments.

## 4 System Design

In this section, we describe our system design. In specific, we will first introduce hardware platform including computation, sensing and communication module. Then, we will present our software architecture to enable safe navigation in unknown environments.



Figure 1. Jackal unmanned ground vehicle

#### 4.1 Hardware Overview.

We chose to use *ClearPath* Jackal Unmanned Ground Vehicle (UGV) as our experimental platform. Jackal is a small field robotics research platform with onboard computer and customizable sensor configuration such as GPS, IMU and LiDAR. It is Robot Operating System (ROS) compatible, so we can quickly test and debug your algorithm in simulation and deploy it to hardware.

**Mobile Platform.** Jackal UGV is a differential drive robot with four equivalent wheels, two on each side running at same speed. The external dimensions are  $508 \times 430 \times 250$  mm. It weighs about 17 kg and can run at top speed 2.0 m/sec.

**Computation, sensing and communication.** Our custom Jackal is equipped with an Intel i7-9700TE CPU with 32GB RAM, an Ouster OS1-32 LiDAR and a UM7 9-axis IMU. This supplies sufficient computation power and sensing capability for autonomous navigation tasks. The UGV can be manually controlled by a Bluetooth joystick or remotely accessed by onboard Wi-Fi. We use the joystick to trigger our problem at the beginning and use it as an emergency stop controller. A local network is setup via a standard router, so we can use visualization tools that come with ROS development kit to monitor running status of our algorithm and save ROS bag for replay and debugging.

#### 4.2 Software Architecture

The software components can be grouped into three categories: Localization and Mapping, Planning and Control. We use Robot Operation System (ROS) as the framework for all high-level tasks running on the robot. Figure 2 is an overview of our system architecture. On the top half, we have the planning block at left and the control modules (in dash rectangular), which are the focus of this paper. We use the out-of-box low-level velocity controller provided by *Clearpath Robotics* which takes linear and angular velocity command and transforms them to motor input signals. In the rest of this section, we will describe the localization and mapping package we used and briefly overview our design in the planning and control.

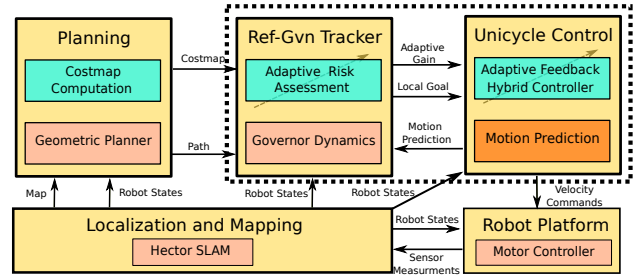


Figure 2. System architecture overview.

**Localization and Mapping.** For localization and mapping task, we use an open-source LiDAR-based 2D SLAM algorithm called Hector SLAM (Kohlbrecher et al. 2011). This algorithm takes 2D laser scan as inputs and outputs robot's poses (position and orientation) in an online constructed occupancy grid map. We use an ROS package named `pointcloud_to_laserscan` to convert 3D pointcloud from Ouster LiDAR to 2D laser scan.

**Planning.** The planning module consists of two parts, a costmap computation block and a standard geometric planner. We choose a classical searched-based planning algorithm named  $A^*$  as our 2D geometric planner. Instead of searching for an optimal path (in terms of travel distance) over binary occupancy grid map, we create a distance-field based costmap as input for the planner. The customizable costmap can be easily tuned to generate optimal paths from max-clearance path to shortest travel distance path, leaving practitioner the freedom to balance safety and efficiency.

**Control.** The control system has two big parts as well, including unicycle control and path tracking. The *unicycle control* module includes an adaptive hybrid controller and a motion predictor. This controller is used to drive a robot from one location to another in free space locally and the motion predictor can compute an outer approximation set of the resulting trajectory connecting these two points. To bridge the gap between a geometric path planner and unicycle controller, we need a path tracker. We create a *environmental-aware reference-governor tracker* that continuously generates proper local goals along the path and sends them to the controller. This tracker estimates running risk by considering local geometric information and system dynamics at the same time. In addition, it also updates an adaptive gain to speed up tracking process when it is safe to do so. Using this tracker, the robot can track the path safely and fast in challenging environments.

## 5 Safe Tracking via Planning-Control Co-Design

This section elaborates the planning, unicycle and reference-governor modules in depth and explains how

planning and control co-design can improve tracking performance yet guarantee safety.

## 5.1 Costmap and Planning

**5.1.1 Costmap Design** A costmap is a representation for the planning search space around a vehicle, it allows planned path to be pushed away from obstacle space (Oleynikova et al. 2016). Inspired by ROS `costmap_2d` package, we design our own costmap curve for the Jackal robot. The footprint of Jackal UGV is approximated as a rectangle with inscribed radius  $r_{ins} = 0.215$  m and circumscribed radius  $r_{cir} = 0.333$  m as shown in Fig. 3a. We set cost for real obstacle and inscribed obstacle (distance to robot center less than inscribed radius) at 19 and the exponential decay rate chosen to be 7.0. To allow robot planning in unknown space yet still prefer known space, we set unknown cell cost at 3. The resulting cost curve is depicted in Fig. 3b. Using the cost curve, we can generate costmap from occupancy grid map message obtained from Hector SLAM. The hector map occupancy grid is first processed as binary image and then pass to `distanceTransform` function provided by OpenCV image processing library. Next, we multiply the distance map (in pixel) by grid map resolution, we get distance map over Euclidean distance metric. Finally, we assign cell cost according to its type and distance and get the costmap. The occupancy grid map and costmap are shown in Fig. 3d.

**5.1.2 Planner Design** In this paper, we modify classical  $A^*$  searched based planning algorithm over 2D grid cell. In specific, we choose heuristic as Manhattan distance and the cost between neighborhood cells on search graph is computed as follows:

$$\text{cost}(\mathbf{p}_1, \mathbf{p}_2) = \|\mathbf{p}_1 - \mathbf{p}_2\| + \text{costmap}(\mathbf{p}_2), \quad (2)$$

where  $\mathbf{p}_1$  and  $\mathbf{p}_2$  are the cell coordinates for parent and child cells and  $\text{costmap}(\mathbf{p}_2)$  denotes the costmap value at  $\mathbf{p}_2$ .

Note that we can set different critical values when generating costmap from occupancy grid map. For example, considering circumscribed radius ( $r_{cir} = 0.333$  m) and map resolution (0.1 m/cell), we can set the obstacle cost lower bound as 5 to ensure resulting path from planner can achieve at least 0.4 m clearance. This critical value 5 can be determined from the cost curve directly, see vertical orange line in Fig. 3b. A comprehensive example can be found in Figure 6 in Sec. 6.1, in which we use different costmap design to generate various paths: from path with shortest travel distance, path with medium travel distance and clearance and path with maximum clearance.

## 5.2 Bi-directional Unicycle Control and Prediction

As mentioned in introduction, an accurate robot trajectory prediction is crucial for robust and fast reference path following. To obtain real-time motion prediction, the author of (İşleyen et al. 2022) proposes several outer approximation sets for robot trajectory in working space. We adopt the ice-cream cone set approximation that outperforms circular reachable set estimation by Lyapunov function. More importantly, this convex cone shape set can be computed efficiently, which makes it a great fit for our task.

When moving obstacle exists, allowing direct backward motion (rather than rotate-and-avoid) can take robot to safer place sooner in certain case. Hence, we extend the forward unicycle controller used in (İşleyen et al. 2022) to be bi-directional and use this controller in experiments with moving obstacles.

**5.2.1 Bi-directional Motion Control** Suppose the robot current state is  $\mathbf{x} = (\mathbf{p}, \theta)$ , given any goal pose  $\mathbf{x}^* = (\mathbf{p}^*, \theta^*)$ , the control law  $\mathbf{u}_{fm}(\mathbf{x}, \mathbf{x}^*) = (v(\mathbf{x}, \mathbf{x}^*), \omega(\mathbf{x}, \mathbf{x}^*))$  is defined as follows,

$$v = k_v e_v \quad \omega = k_\omega \text{atan}(e_v^\perp / e_v). \quad (3)$$

where  $k_v > 0$  and  $k_\omega > 0$  are control gains for linear and angular velocities and  $e_v$  and  $e_v^\perp$  are define as follows\*:

$$e_v = \begin{bmatrix} \cos \theta \\ \sin \theta \end{bmatrix}^\top (\mathbf{p}^* - \mathbf{p}), \quad e_v^\perp = \begin{bmatrix} -\sin \theta \\ \cos \theta \end{bmatrix}^\top (\mathbf{p}^* - \mathbf{p}). \quad (4)$$

One can show that unicycle model (1) controlled by (3) is globally asymptotically stable (İşleyen et al. 2022, Lemma 1) in position, i.e., for any  $\mathbf{p}^*$ , the closed-loop unicycle trajectory  $\mathbf{p}(t)$  satisfies  $\lim_{t \rightarrow \infty} \mathbf{p}(t) = \mathbf{p}^*$ .

**5.2.2 Reachable Set Prediction** Given robot position and goal location, we can construct an ice cream cone shape outer approximation of its reachable set enclosing robot future trajectory. An illustrative example given in Fig. 4, where the cone is depicted in orange with red and green stars denoting start and goal locations.

**Proposition 1.** For any given goal  $\mathbf{x}^* = (\mathbf{p}^*, \theta^*)$  and any initial condition  $\mathbf{x}_0 = (\mathbf{p}_0, \theta_0)$ , the closed-loop trajectory  $\mathbf{x}(t) = (\mathbf{p}(t), \theta(t))$  under control law (3) is positional positively invariant in the ice-cream-cone-shape motion prediction set  $\mathcal{M}(\mathbf{x}, \mathbf{p}^*)$  that is defined as

$$\mathcal{M}(\mathbf{x}, \mathbf{p}^*) := \mathcal{C}(\mathbf{p}, \mathbf{p}^*, \|e_v^\perp\|) \quad (5)$$

\*To resolve the indeterminacy, set  $\omega = 0$  when  $\mathbf{p} = \mathbf{p}^*$ .

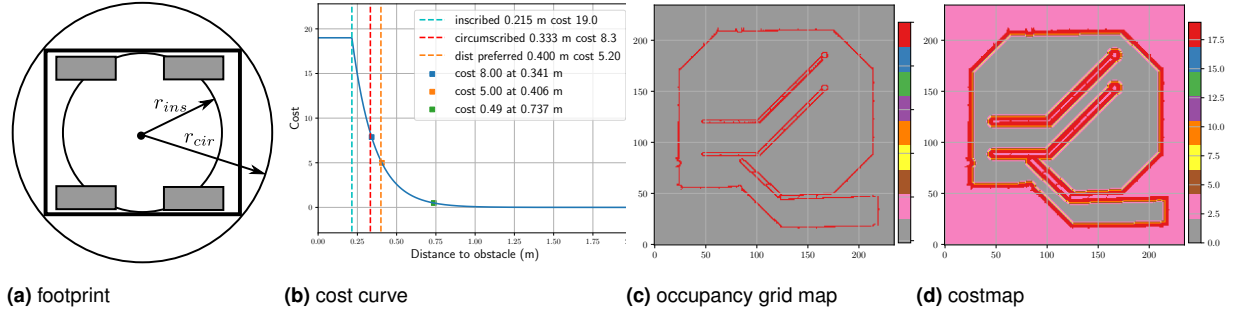


**Figure 3.** Jackal robot cost curve design. The robot footprint is approximated as a rectangle with inscribed radius  $r_{ins} = 0.215$  m and circumscribed radius  $r_{cir} = 0.333$  m as depicted in (a). Cost curve design for Jackal robot is shown in (b) where lethal obstacle and inscribed cost is set to 19 with decay rate 7.0. The occupancy grid map of Jackal Race simulated world is shown in (c) with cell value being the probability (in percent) being occupied by obstacles. A corresponding costmap is shown in (d), in which cell value stands for traversing cost.

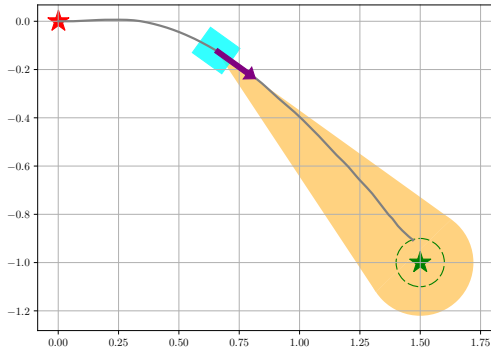


**Figure 4.** Cone shape reachable set prediction. The start and goal are depicted as red and green stars respectively with green circle being the goal region. The robot is scaled and printed as cyan rectangular with purple arrow showing its instantaneous moving direction. The ice-cream shape reachable set is shown in orange.

where the bounded ice-cream cone  $\mathcal{C}(\mathbf{p}, \mathbf{p}^*, \rho)$  is defined as

$$\mathcal{C}(\mathbf{a}, \mathbf{b}, r) := \{\mathbf{a} + \alpha(\mathbf{z} - \mathbf{a}) \mid \alpha \in [0, 1], \mathbf{z} \in \mathcal{B}(\mathbf{b}, r)\}, \quad (6)$$

and  $\mathcal{B}(\mathbf{c}, r) := \{\mathbf{z} \in \mathbb{R}^2 \mid \|\mathbf{z} - \mathbf{c}\| \leq r\}$  is the Euclidean closed ball centered at  $\mathbf{c} \in \mathbb{R}^2$  with radius  $r \geq 0$ .

**Proof.** The proof follows from Proposition 4 of (İşleyen et al. 2022).

To help later discussion, we named control law (3) as *cone controller*. Note that, this controller only guarantees position convergence, orientation alignment is not enforced.

### 5.3 Reference Governor Safe Tracker

In this section, we will present the most important part of our integrated planning and control co-design, i.e., the reference governor tracker. This module handles safety risk estimation and generates local goals to unicycle control block. In this part, we will first introduce our adaptive risk assessment module followed by governor dynamics for static environment. Next, to enable the tracker to work in presence of moving obstacles, we propose a new active tracker by embedding safe constraints using control barrier functions. Finally, we summarize our navigation algorithm.

#### 5.3.1 Adaptive Risk Assessment and Directional Boost

By jointly considering bi-directional feed-forward (costmap) and feedback information (motion prediction), we define a safety/risk metric using the distance between motion prediction set and obstacle set defined over costmap:

$$d(\mathcal{M}(\mathbf{x}, \mathbf{p}^*), \mathcal{O}^+), \quad (7)$$

where  $\mathcal{O}^+$  is the inflated obstacle space defined over costmap and  $d(\mathcal{A}, \mathcal{B})$  denotes metric associated with Euclidean norm. As mentioned in Sec. 5.1.1, a practitioner can design different cost curves and compute corresponding  $\mathcal{O}^+$  as needed. Note that, this safety metric considers not only robot motion, but also its surrounding local environment. Our tracker uses it to decide how fast the robot tracking a path adaptively without solving complicated optimization online to get time-parameterized trajectory online.

Moreover, to achieve proper directional risk assessment as a smart agent, we embed the robot's running state and surrounding environment into our risk metric design. Inspired by (Li et al. 2020), we develop a boost gain for longitudinal motion by computing the ratio of directional safety metric and regular one. With this gain, robot can go fast under straight motion in long corridor-like passages.

First, let us recall the definition of quadratic norm and state-dependent direction metric. A quadratic norm induced by  $\mathbf{Q} \in \mathbb{S}_{>0}^n$  will be denoted by  $\|\mathbf{v}\|_{\mathbf{Q}} := \sqrt{\mathbf{v}^\top \mathbf{Q} \mathbf{v}}$ . Define distance from a set  $\mathcal{A}$  to a set  $\mathcal{B}$  using quadratic norm as follows:

$$d_{\mathbf{Q}}(\mathcal{A}, \mathcal{B}) := \inf_{\mathbf{a} \in \mathcal{A}, \mathbf{b} \in \mathcal{B}} \|\mathbf{a} - \mathbf{b}\|_{\mathbf{Q}}. \quad (8)$$

Standard Euclidean distance is a special case of quadratic norm based with  $\mathbf{Q} = \mathbf{I}$ . For simplicity, we use  $\|\mathbf{v}\|$  and  $d(\mathcal{A}, \mathcal{B})$  denotes metric associated with Euclidean norm. To embed directional preference in distance metric, we need a special  $\mathbf{Q}$  called directional matrix that defined as follows:

**Definition 2.** (Li et al. 2020, Def. 2) A *directional matrix* associated with elongated vector  $\mathbf{v}$  and scalars  $c_2 > c_1 > 0$  is defined as

$$\mathbf{Q}[\mathbf{v}] = \begin{cases} c_2 \mathbf{I} + (c_1 - c_2) \frac{\mathbf{v} \mathbf{v}^\top}{\|\mathbf{v}\|^2}, & \text{if } \mathbf{v} \neq \mathbf{0}, \\ c_1 \mathbf{I}, & \text{otherwise.} \end{cases} \quad (9)$$

In specific, we use directional matrix  $\mathbf{Q}[\mathbf{v}]$  as Q-norm kernel and set robot heading as elongated direction, i.e.,  $\mathbf{v} = [\cos \theta, \sin \theta]^\top$ . Then, the SDDM-based boost gain can be defined as:

$$\beta := \begin{cases} \frac{d_{\mathbf{Q}[\mathbf{v}]}(\mathcal{M}(\mathbf{x}, \mathbf{g}), \mathcal{O}^+)}{d(\mathcal{M}(\mathbf{x}, \mathbf{g}), \mathcal{O}^+)} & \text{if } d(\mathcal{M}(\mathbf{x}, \mathbf{g}), \mathcal{O}^+) > 0 \\ 1 & \text{otherwise} \end{cases} \quad (10)$$

to speed up the longitudinal motion (3), i.e.,  $v = \beta k_v e_v$ .

*Remark 1.* The SDDM-based boost gain  $\beta$  is uniformly bounded. Following the proof of (İşleyen et al. 2022), one can verify that the shape of cone-shape motion prediction  $\mathcal{M}(\mathbf{x}, \mathbf{g})$  does not change if boost gain  $\beta > 0$ .

**5.3.2 Governor Control Policy Design** In this section, we show how to use adaptive risk developed above to construct two reference governor trackers for path following. We will first introduce the a reference governor tracker design with necessary backgrounds. This tracker can help a robot navigate fast and efficiently in static environments. To handle moving obstacles, we change the governor dynamics allowing it to follow a safer goal around the given path but not necessarily on it. This extension can help the robot navigate safely in challenging situations with multiple obstacles. Controlled by our algorithm, the robot can progress to the goal efficiently while actively avoiding incoming obstacles in a natural way.

A reference governor is a virtual first-order dynamical system defined as follows:

$$\dot{\mathbf{g}} = -k_g(\mathbf{g} - \mathbf{g}^*), \quad (11)$$

where  $\mathbf{g} \in \mathbb{R}^2$  is the internal governor states and  $\mathbf{g}^* \in \mathbb{R}^2$  is input signal to be determined. The governor state  $\mathbf{g}$  is used to guide robot dynamics while following input signal  $\mathbf{g}^*(t)$  served as intermediate goals along the reference (path  $\mathcal{P}$ ). To utilize a reference governor for path following, we need a dynamic safety margin (DSM) (Nicotra and Garone 2018) for collision avoidance constraints. A dynamic safety margin serves as an indicator of system safeness, wherein a larger value of it signifies increased safety. As shown in (İşleyen et al. 2022) and (Li et al. 2020), the distance between reachable set (projection on working space) and obstacle space is a suitable candidate.

**Lemma 1.** For  $\mathbf{g} \in \text{Int}(\mathcal{F})$ , the  $\mathbf{g}$ -parameterized function

$$\Delta E(\mathbf{x}, \mathbf{g}) := d(\mathcal{M}(\mathbf{x}, \mathbf{g}), \mathcal{O}^+), \quad (12)$$

is a *dynamic safety margin*.

Next step is to find local goals used in governor dynamics, i.e.,  $\mathbf{g}^*$  in (11). Using safety margin  $\Delta E$ , we can define a *local safe zone*, from which local goals will be computed. Then we can compute *local projected goal* as input signal  $\bar{\mathbf{g}}$ . The definitions of local safe zone and local projected goal are presented below with an illustrative plot in Fig. 5.

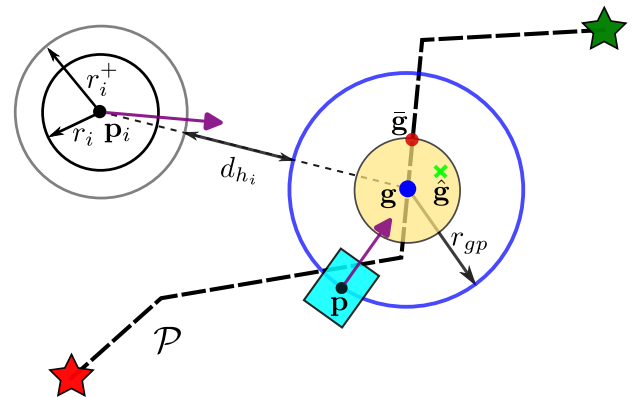


**Figure 5.** Geometric relationship of local safe zone  $\mathcal{LS}$  (yellow ball), local projected goal  $\bar{\mathbf{g}}$  (red dot) and optimized local projected goal  $\hat{\mathbf{g}}$  (green dot).

**Definition 3.** A *local safe zone* is a time-varying set, determined by the joint system-governor state  $(\mathbf{x}, \mathbf{g})$ , a dynamic safety margin  $\Delta E(\mathbf{x}, \mathbf{g})$ ,

$$\mathcal{LS}(\mathbf{x}, \mathbf{g}) := \{\mathbf{q} \in \mathbb{R}^2 \mid \|\mathbf{q} - \mathbf{g}\|^2 \leq \Delta E(\mathbf{x}, \mathbf{g})\}. \quad (13)$$

**Definition 4.** A *local projected goal* at system-governor state  $(\mathbf{x}, \mathbf{g})$  is a point  $\bar{\mathbf{g}} \in \mathcal{LS}(\mathbf{x}, \mathbf{g})$  that is furthest along the reference path  $\mathcal{P}$ :

$$\bar{\mathbf{g}} = \mathcal{P}(\bar{\sigma}), \quad \bar{\sigma} = \operatorname{argmax}_{\sigma \in [0,1]} \{\sigma \mid \mathcal{P}(\sigma) \in \mathcal{LS}(\mathbf{x}, \mathbf{g})\}. \quad (14)$$

Till now, we have completed the first reference-governor based path tracker. Combining unicycle controller (3) and governor dynamics (11) with time-varying input signal  $\mathbf{g}^*(t) = \hat{\mathbf{g}}$  in governor dynamics, we have the robot-governor dynamics:

$$\dot{x} = \beta v \cos \theta \quad (15a)$$

$$\dot{y} = \beta v \sin \theta \quad (15b)$$

$$\dot{\theta} = \omega \quad (15c)$$

$$\dot{\mathbf{g}} = -k_g(\mathbf{g} - \bar{\mathbf{g}}), \quad (15d)$$

where  $\beta$  is the SDDM boost gain in (10).

**Theorem 1.** *Given a reference path  $\mathcal{P}$ , consider the closed-loop system in (15). Suppose that the initial state  $(\mathbf{x}_0, \mathbf{g}_0)$  satisfies:*

$$\Delta E(\mathbf{x}_0, \mathbf{g}_0) > 0, \quad \mathbf{g}_0 = \mathbf{p}(0) \in \mathcal{F}, \quad (16)$$

where  $\Delta E(\mathbf{x}, \mathbf{g}) = d(\mathcal{M}(\mathbf{x}, \mathbf{g}), \mathcal{O}^+)$ . Then, the robot converges to goal region close to  $\mathcal{P}(1)$  without collision, i.e.,  $\mathbf{p}(t) \in \mathcal{F}, \forall t \geq t_0$ .

The reference governor tracker now can guide robot navigate in static unknown environment safely and efficiently. When moving obstacle approaches to the robot ( $\Delta E = 0$ ), robot will stop in place and resume its motion to goal when moving obstacles leaves ( $\Delta E(t) > 0$ ). However, the non-at-fault stop-and-go strategy may not be efficient enough in certain applications where robots are required to navigate through crowds all the time. To overcome this drawback, we extend our algorithm in the following section.

#### 5.4 Governor Control Policy Extension for Moving Obstacles

Merely adhering to the planned path is insufficient for promptly avoiding approaching obstacles. An intelligent algorithm should grant the robot the ability to temporarily deviate from the predetermined path and execute emergency maneuvers when deemed necessary. To acquire such capability, we not only need to bi-directional low-level motion control, but the leading signal shall also be flexible to provide proper guidance. The unicycle controller (3) shown in 5.2 already allows bi-direction movement. To satisfy the second requirement, we propose an optimization-based method to modify the input signal ( $\bar{\mathbf{g}}$ ) in governor dynamics (11), allowing the governor to pursue local goals that deviate from given path. So, when moving obstacles endanger robot's progression, it can actively take proper avoidance maneuver in a defensive fashion.

To ease the discussion, let us suppose there are  $k$  moving obstacles with circular shape centered at location  $\{\mathbf{p}_i\}_{i=1}^k$  with radius  $\{r_i\}_{i=1}^k$ . All agent behave like an independent, linear, time-invariant system satisfying the

following dynamics:

$$\dot{\mathbf{p}}_i = \mathbf{v}_i, \quad (17)$$

where  $\mathbf{v}_i$  is the velocity of agent  $i$ . For simplicity, we assume the position and velocity of moving agents are known to the robot. In practice, this information are readily available from front-end perception module. Inspired by safety control techniques used by control barrier function (CBF) (Ames et al. 2019), we formulate a convex optimization problem to shift governor input reference signal  $\bar{\mathbf{g}}$  in a minimally invasive way to avoid incoming moving agents.

**CBF construction for moving obstacle.** Let  $r_i^+ = r_i + r_{cir}$  be the inflated radius of moving obstacle  $i$ , define the gap between two balls  $\mathcal{B}(\mathbf{p}_i, r_i^+)$  and  $\mathcal{B}(\mathbf{g}, \|\mathbf{p} - \mathbf{g}\|)$  as:

$$d_{hi} := \|\mathbf{g} - \mathbf{p}_i\| - \|\mathbf{g} - \mathbf{p}\| - r_i^+ \geq 0.$$

The gap between these two balls can be visualized at Figure. 5. One can prove that the cone motion prediction set  $\mathcal{M}(\mathbf{x}, \mathbf{g})$  is a subset of the ball  $\mathcal{B}(\mathbf{g}, \|\mathbf{p} - \mathbf{g}\|)$ , i.e.,

$$\mathcal{M}(\mathbf{x}, \mathbf{g}) \subset \mathcal{B}(\mathbf{g}, \|\mathbf{g} - \mathbf{p}\|), \quad (18)$$

see detail at (İşleyen et al. 2022, Prop.8). Hence, the gap  $d_{hi}$  can be considered as a DSM between moving agent  $i$  and the robot. Therefore, we can construct CBF for agent  $i$  from  $d_{hi}$ :

$$h_i(\mathbf{x}, \mathbf{g}, \mathbf{p}_i) = \|\mathbf{g} - \mathbf{p}_i\|^2 - (r_i^+ + \|\mathbf{g} - \mathbf{p}\|)^2. \quad (19)$$

To enforce collision avoidance constraints, the CBF constraint becomes:

$$\dot{h}_i(\mathbf{x}, \mathbf{g}, \mathbf{p}_i) \geq -\alpha_i(h_i(\mathbf{x}, \mathbf{g}, \mathbf{p}_i)), \quad (20)$$

where  $\alpha_i(\cdot)$  is a class- $\mathcal{K}$  function to be designed. Expand out the expression of  $\dot{h}$ , we have

$$\dot{h}_i(\mathbf{x}, \mathbf{g}, \mathbf{p}_i) = \frac{\partial h_i}{\partial \mathbf{g}} \mathbf{u}_{\mathbf{g}} + \frac{\partial h_i}{\partial \mathbf{p}} \mathbf{u} + \frac{\partial h_i}{\partial \mathbf{p}_i} \mathbf{v}_i, \quad (21)$$

where  $\mathbf{u} = [k_v e_v \beta \cos \theta, k_v e_v \beta \sin \theta]^\top$  is the control signal of robot and  $\mathbf{u}_{\mathbf{g}} \in \mathbb{R}^2$  is the governor control to be determined.

**Local projected goal modification.** With the above CBF for moving obstacle, we can use them to push local projected goal  $\bar{\mathbf{g}}$  away from path  $\mathcal{P}$  temporarily if the nearest obstacle is getting too close to the robot. Let  $h^* := \min_i h_i$ , we can formulate the optimization problem as follows:

$$\min_{\mathbf{u}_{\mathbf{g}} \in \mathbb{R}^2, \hat{\mathbf{g}} \in \mathbb{R}^n} \|\hat{\mathbf{g}} - \bar{\mathbf{g}}\|^2 \quad (22a)$$

$$\text{subject to } \dot{h}^* \geq -\alpha_i(h^*) \quad (22b)$$

$$\mathbf{u}_{\mathbf{g}} = -k_g(\mathbf{g} - \hat{\mathbf{g}}) \quad (22c)$$

$$\hat{\mathbf{g}} \in \mathcal{LS}(\mathbf{x}, \mathbf{g}). \quad (22d)$$



This optimization problem tries to search a modified local projected goal  $\hat{\mathbf{g}}$  within local safe zone  $\mathcal{LS}(\mathbf{x}, \mathbf{g})$  that is close to the original one  $\bar{\mathbf{g}}$ . When moving obstacle endangers robot operation, it will push the projected goal away from path  $\mathcal{P}$  to reduce collision risk. An illustrative example is depicted in Fig. 5, where the optimized projected goal  $\hat{\mathbf{g}}$  (green dot) is found in the vicinity of local projected goal  $\bar{\mathbf{g}}$  (red dot) to avoid nearest incoming obstacle.

It is not hard to verify that this optimization problem is a convex program so it can be solved efficiently by solvers that support quadratic-constrained quadratic program (QCQP). Replacing  $\bar{\mathbf{g}}$  with modified projected goal  $\hat{\mathbf{g}}$  in (15d), i.e.,

$$\dot{\mathbf{g}} = -k_g(\mathbf{g} - \hat{\mathbf{g}}), \quad (23)$$

we get the new robot-governor controller that can drive robot safely among moving obstacles. The effective of this new active robot-governor control policy are verified in both simulation and hardware in experiment in Sec. 6.5. For easy reference, we call this optimization-based extension described in (22) and (23) **active governor control policy**.

*Remark 2.* In static environment, the proposed algorithm is provably safe. When moving obstacles exist, the safety requirement is more involved and we validate the effective of our algorithm in hardware experiments.

## 6 Evaluation

In this section, we will evaluate the performance of our path-following controller. We will start our evaluation for individual components in our system architecture. Then we will test the overall performance of our controller using both simulations and hardware demonstrations. For all simulated experiments, we plot a 2D planning path as a black dash line with start and goal denoted by a red and green star, respectively. The velocity profiles are shown as magenta arrows perpendicular to the robot path.

**Experiment Setup and Parameters.** In this section, all experiments share the same design parameters and control gains unless explicitly pointed out. For localization and mapping, the hector SLAM packages provide robot pose estimation at about 20 Hz with 0.1 m positional and 0.1 rad angular accuracy. The map resolution is chosen at 0.1 m. The control gains and directional matrix parameters are summarized in Table 1.

**Table 1.** Parameter table of control gains.

Parameter	$k_g$	$k_v$	$k_\omega$	$\gamma_i$	$c_1$	$c_2$
Value	2.0	0.5	1.5	0.2	1	9

Unless pointed out explicitly, all experiments share the same control parameters in this table. The class- $\mathcal{K}$  function

for moving obstacle experiment is defined as follows:

$$\alpha_i(h_i) = \gamma_i h_i^2. \quad (24)$$

### 6.1 Costmap Design for Planning and Safe Control

From previous discussion in Sec. 5.1 and 5.3.1, we know that costmap can affect the planner's performance and safety metric estimation. Using different cost curve designs, we can control path clearance. In this section, we want to demonstrate how our algorithm can be tailored for different preferences.

Given map resolution and robot circumscribed radius, we choose 0.4 m as the minimum path clearance for all cost curve designs. Planning cutoff value and obstacle lower bound can be computed from cost curve. For example, for medium clearance design whose cost curve is depicted in Fig. 3b, we set planning cutoff value as 5 (corresponding to 0.406 m clearance) and obstacle lower bound as 8 (corresponding to 0.333 m clearance). Similarly, we design another two cost curves for minimum clearance path (shortest path with desired 0.4 m clearance) and maximum clearance path. The critical values of these three costmap designs are listed in Table 3.

Using these different costmap designs, three corresponding paths are computed in Jackal race world and depicted as black dash line as shown in Fig. 6. For all cases, our algorithm can safely drive the robot towards goal. The resulting robot paths are plotted using colored line where robot to obstacle distance is embedded by gradient color<sup>†</sup>. Associated quantitative results are summarized at Table. 2. From which, we can see choosing the shortest planned path does not mean reaching the goal faster. The medium and maximum clearance options both achieve the goal faster by taking safer routes.

### 6.2 SDDM Boost on C-shape Environments

To demonstrate the effective of directional boost gain (10) derived in last section, we create a C-shape simulated environment using Gazebo with hand-picked path (black dashed line) as shown in Fig. 7. Two controllers are tested: left (boost gain disable, i.e.,  $\beta \equiv 1$ ); right (boost gain enabled). All other configurations remain the same. The boost gain value can be read from the color bar on the side. From the plots, we see that the robot with SDDM boost speeds up faster in straight line and remains low speed at turns, while the other one being overly cautious. As a result, the controller with boost gain finishing the task only uses 2/3 time of the other one.

<sup>†</sup>The value of color bar is saturated at 1 for visibility.

**Table 2.** Simulation quantitative result of three costmap designs.

Costmap Design	Plan Path Length	Robot Traj. Length	Finished Time	Avg. Clearance	Min. Clearance
minimum clearance	15.10 m	15.66 m	32.80 sec	0.45 m	0.13 m
medium clearance	16.19 m	15.63 m	20.62 sec	0.63 m	0.34 m
maximum clearance	22.28 m	20.32 m	18.96 sec	1.31 m	0.38 m

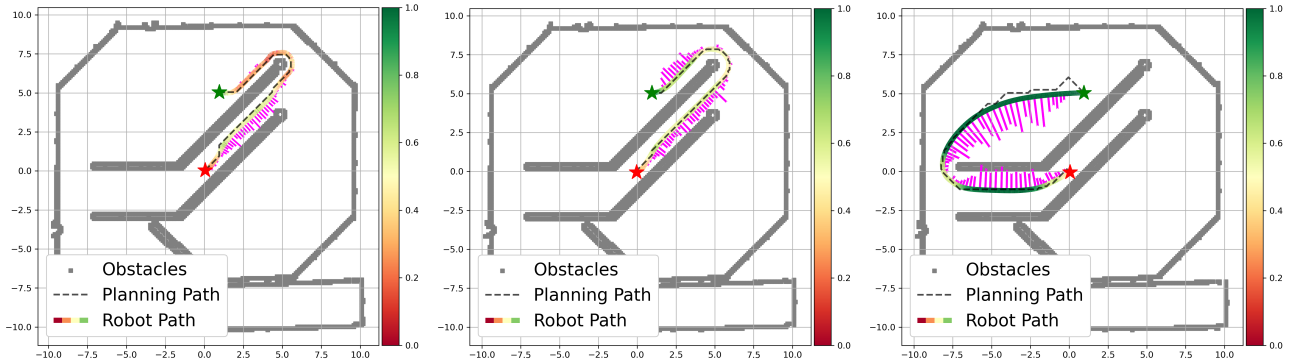


**Figure 6.** Jackal race world ROS simulation with three different cost curve designs.

**Table 3.** Costmap Design Parameters.

Costmap Design	Decay Rate	Planning Cutoff	Obstacle Lower Bound
minimum clearance	15.0	1	3
medium clearance	7.0	5	8
maximum clearance	1.0	15	17

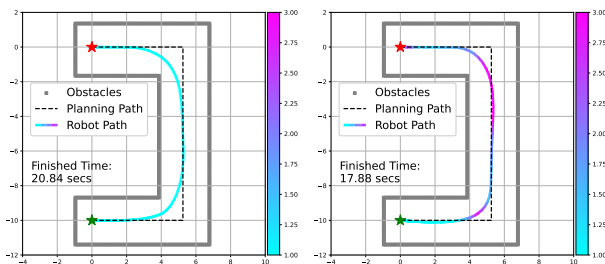


**Figure 7.** Simulation of robot-governor path following controller in C-shape environment. The adaptive boost gain is disable at left and enabled at right.

### 6.3 Baseline Comparison

In this section, we compare our work with a recent work called EVA-Planner, in which an environmental-aware adaptive planner is developed using MPC techniques with novel SDF gradient based directional safety metric. Two experiments have been done to compare these two methods with emphasis on difference on safety and adaptivity, respectively. The EVA planner solves the planning and control problem via a two-layer hierarchy MPC, all constraints are encoded as soft cost and solved by a gradient-based numerical solver (NLopt<sup>‡</sup> + L-BFGS algorithm). It is worth pointing out that the EVA planner tries to solve are constrained nonlinear non-convex

optimization problems. Therefore, the optimality and safety constraints satisfactions are not guaranteed. We tried our best to fine-tune it.

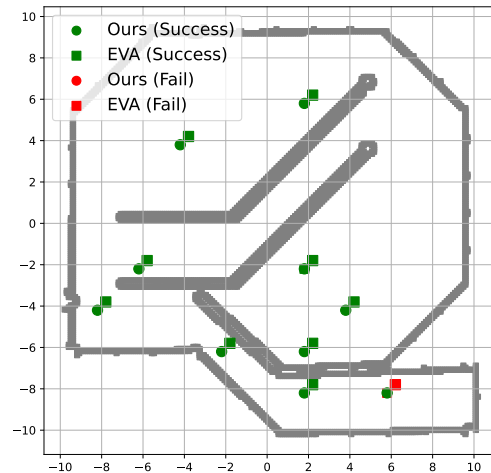


**Figure 8.** Safety test on ten random selected goals.

**Safety Ten Point Test.** In the first experiment, we randomly sampled ten feasible points from Jackal race world as shown in Fig. 6. All goals are at integer grid

<sup>‡</sup><http://github.com/stevengi/nlopt>

intersections, markers positions are shifted slightly for visualization. From the plot, we can see that our algorithm can reach all ten goals safely, while EVA planner failed to reach one goal at  $(6, -8)$ . In our implementation, the EVA planner failed to find global optimal solution of the high MPCC optimization problem and outputs trajectory go through obstacles. Other paper find out that this EVA planner performance degrades (collision rate gets higher) when robot operates in environment with high obstacle density (Liu et al. 2023).

**Adaptivity Maze Test.** In the second experiment, we create a challenging maze-like environment to test the adaptivity of these two methods. The robot is asked to go from the start position at origin to goal at  $(6, 6)$  in the maze center. To accomplish this task, the robot must go through corridors that become narrower from outer (about 3m wide) to inner (less than 1 m wide). For both methods, we use the same 0.4 m inflation radius in A\* planner. The low MPC used in EVA planner are set similar distance (0.7 m) clearance preference as our medium clearance cost curve design. Both methods use the same parameters as in Jackal race world. The results are shown in Fig. 9. The velocity profiles are depicted perpendicular along robot paths using purple lines (longer faster). The safety distance margin  $d(\mathbf{p}, \mathcal{O}^+)$  is embedded in colorbar. As we can see from this plot, our method accomplishes this task successfully while adapting its speed according to local environments, i.e., faster when corridor is wide and slower when it becomes narrower. In contrast, the EVA planner cannot handle this task elegantly using the same hyper-parameters. Although the EVA planner runs faster at beginning when corridor is wide, the two cost terms of progress (pushing robot progress along planned path) and direction safety metric (reducing speed when robot getting closer to obstacle) are fighting each other when robot getting deep in the maze. This results in wobbly motion and snake trajectory, and eventually drive robot crash to wall.

#### 6.4 Hardware Demonstration in Clutter Unknown Environment

In this experiment, we test our algorithm in a large scale ( $40 \times 20$  m) office-like collaborative lab environment. The place is shared with multiple research lab groups with various robots, complex experiment platform, package boxes, working desks, etc., as shown in Fig. (10a)-(10c). During this experiment, we use RViz to specify a few goals over unknown regions and let the robot explore autonomously. This experiment takes about 10 minutes, a first-person video captured by onboard GoPro camera can be found at [here](#). While exploring this place, the robot creates costmap online through occupancy grid and navigate itself safely without any collision. The experiment overview can be found in Figure. 10, where the final

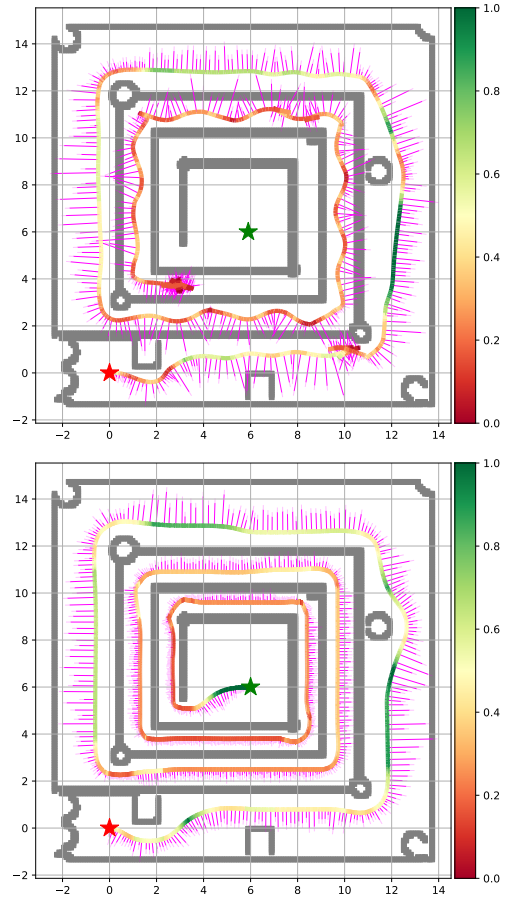


**Figure 9.** The result maze adaptivity experiment. The distance from robot to inflated obstacle space is embedded in robot path. The value of colorbar is saturated at 1 m for better visualization.

costmap is depicted in plot (d). Three local scenes (marked in green boxes) are shown in the top row subplot (a)-(c) with associated quantitative results right down each of them.

The robot cruise speed adapts to sensed local environments, slowing down when entering obstacle-dense areas and speed up when in wide open spaces as shown in these plots as shown all scenes. From the middle row plots, we can see that the speed of Jackal robot (orange curve) is higher when it is distance to obstacle (green line) is bigger. The adaptive directional SDDM boost (purple curve) increases when motion direction is aligned with local environments. This can be seen clearly in scene (2) in Fig. (10b) when robot tries to go through a long narrow aisle. It allows robot maintains relatively high speed in straight motions and slows down when turn-and-go are required to pass obstacles (red luggage in front and green chair at behind) in the midway.

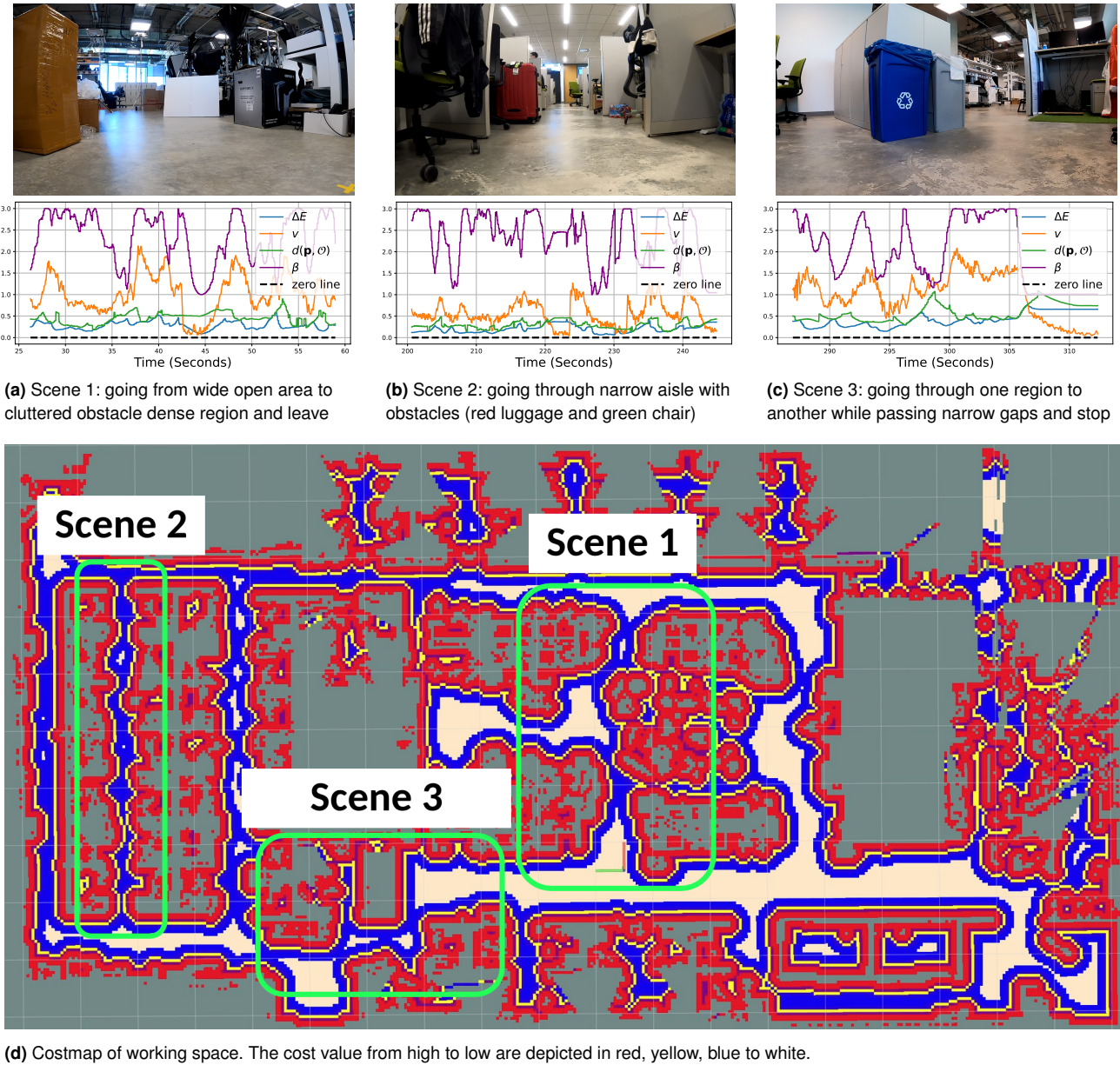


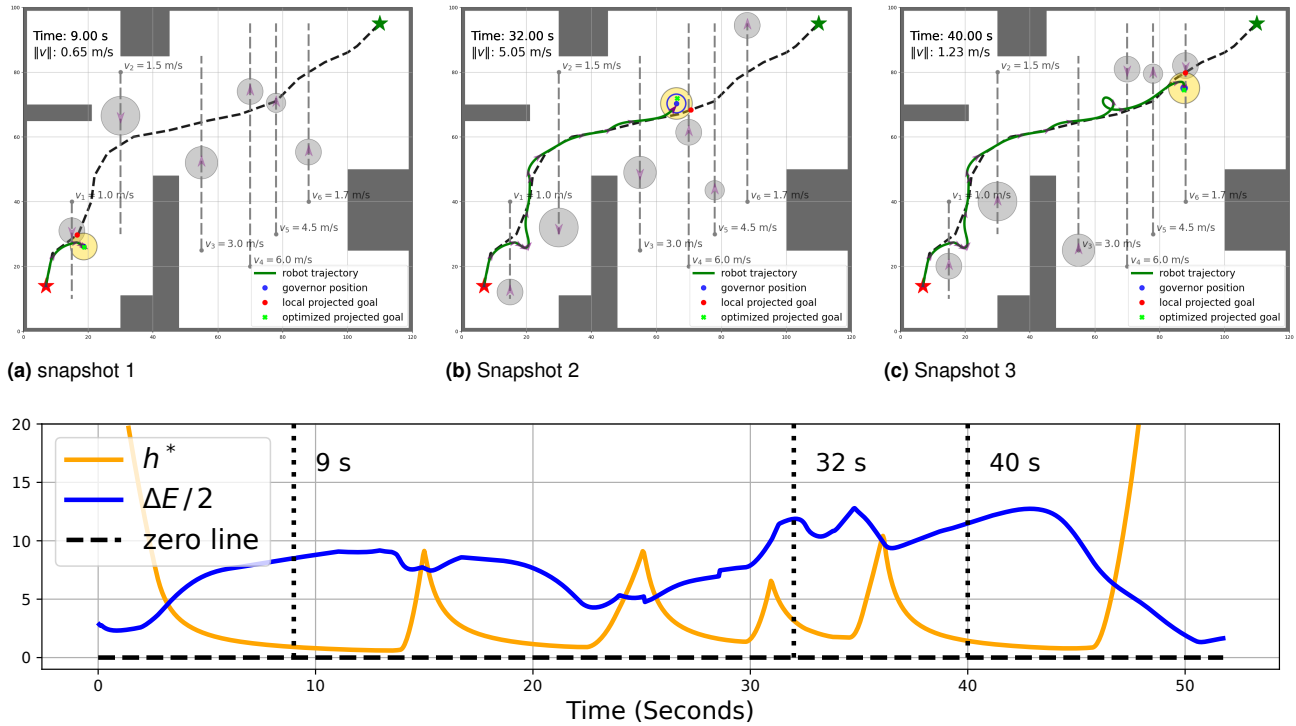
**Figure 10.** Hardware experiment in a large-scale (about  $40\text{ m} \times 20\text{ m}$ ) collaborative working space. Three representative scenes are marked on final costmap (d) using green boxes. At top row, photos of these three scenes are shown with associated quantitative plots.

### 6.5 Moving Obstacles Experiments

In this section, we will evaluate the path tracker extension using the active governor control policy. We will test the performance of our controller in dynamically changing environments with moving obstacles. The position and velocity information of moving agents are assumed to be known to the robot. For simulated experiments, the trajectories of moving obstacles are calculated ahead and

replayed at runtime. For hardware demonstration, we use Vicon motion capture system to track motions of human actors and then pass this information to Jackal robot over wireless network.

**Simulation experiment.** In this experiment, the robot is asked to follow a predefined path (black dash line) while avoiding six known moving obstacles (light gray circles) with different size and running speed. See snapshot in



(d) Safe metric for static (blue curve) and moving obstacle (organ curve).

**Figure 11.** Summary of moving obstacle simulation with six dynamic obstacles at different running speed and sizes. When incoming obstacle endangers robot motions, the CBF constraints become active and push optimized local projected goal (green cross) away from local projected goal (red dot) allowing robot to take necessary defensive maneuvers.

Fig. 11b for the simulation setup. Control parameters used in this experiment are summarized in Table 4. To handle fast moving obstacles, we use more conservative circular shape motion prediction set, i.e.,  $\mathcal{B}(\mathbf{g}, \|\mathbf{g} - \mathbf{p}\|)$  (blue circle) and increased control inputs bounds to  $[-10, 10]$  m/sec and  $[-4, 4]$  rad/s for linear and angular velocities, respectively. Three snapshots of this simulation are shown in Fig. 11. The resulting robot trajectory is depicted as a green line with purple arrows indicating its heading. Using active governor control policy in Sec. 5.4, we allow local projected goal to deviate from path temporarily, so robot can take necessary defensive maneuvers to avoid nearby incoming obstacles and quickly resume to normal path following behavior when is safe to do so.

**Table 4.** Parameter table of control gains used in moving obstacle simulation.

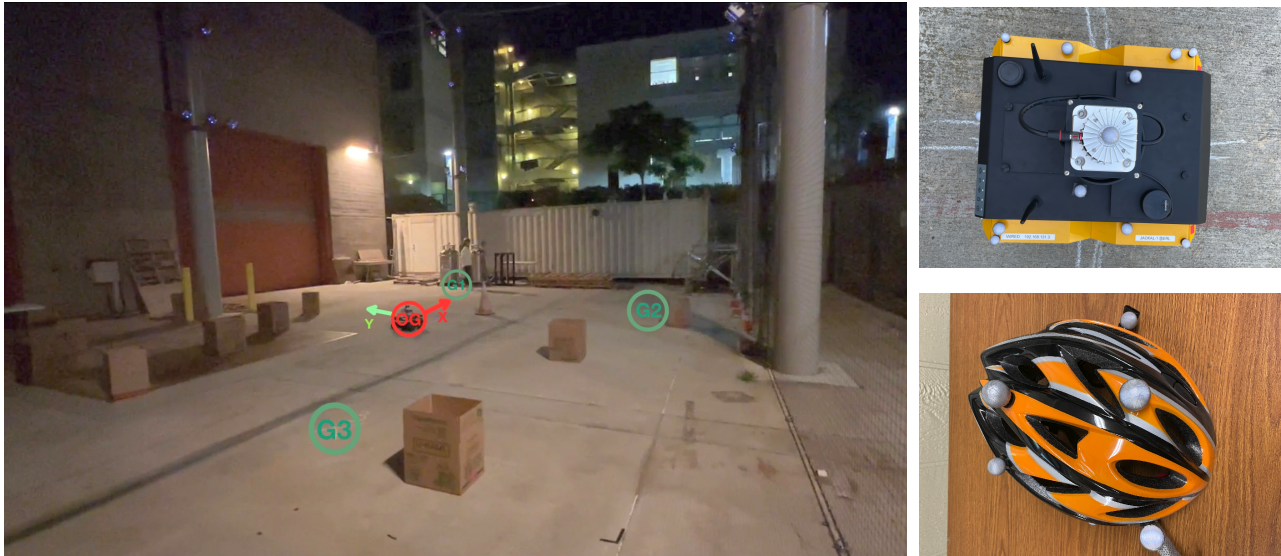
Parameter	$k_g$	$k_v$	$k_\omega$	$\gamma_i$	$c_1$	$c_2$
Value	2.0	2.0	5.0	0.15	1	1

**Hardware experiment.** The site setup is shown in Fig. 12a with static obstacles (boxes, walls, pillars, etc.,) and moving

obstacles (two actors wearing helmets). The robot is asked to go through three different goals (marked as green circle) and return to origin (red circle). The robot does not have any prior information of this environment, except receiving moving obstacle positions from Vicon system. Actors are instructed to interrupt robot motions to each goal but not being adversarial against it. Same controller parameter set are used as in Table. 1. Please check out experiment video at [here](#) for better visualization. From the bottom plot 12c, we see that the robot remains safe during the whole experiment (blue and purple line above zero).

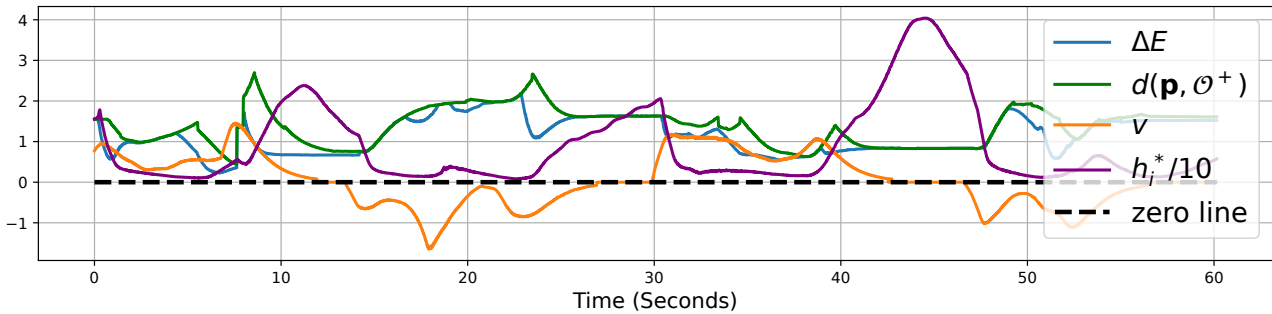
## 7 Conclusion

This paper presented an environmental adaptive and safe path-following tracker via planning and control co-design. Through the usage of custom A\* planner over costmap, directional safety metric and conic shape motion prediction, our reference governor based path tracker can achieve safe and efficient safe navigation in challenging large-scale unknown environments. The effectiveness and adaptability are verified in various simulated and real experiments. By further integrating with control barrier function, our



(a) experiment site with Vicon motion capture system

(b) robot and helmet with markers



(c) safe metric for static and moving obstacle

**Figure 12.** Hardware experiment with Jackal robot and two moving obstacle. Actors' positions are captured by Vicon motion captures system and passed to the robot via local network. This robot re-plans at about 10 Hz online to reach different goals while avoiding moving pedestrians temporarily crossing the path. Video is available at [here](#).

method can handle dynamic environments with moving obstacles under mild assumption. Future work will focus on extending planner to be  $SE(2)$  space and developing semantic mapping algorithm can auto detect moving obstacles onboard.

### Funding

We gratefully acknowledge support from NSF CRII IIS-1755568, ARL DCIST CRA W911NF-17-2-0181, and ONR SAI N00014-18-1-2828.

### References

Ames AD, Coogan S, Egerstedt M, Notomista G, Sreenath K and Tabuada P (2019) Control barrier functions: Theory and

applications. In: *IEEE European Control Conference (ECC)*. pp. 3420–3431.

Ames AD, Xu X, Grizzle JW and Tabuada P (2017) Control barrier function based quadratic programs for safety critical systems. *IEEE Transactions on Automatic Control (TAC)* 62(8): 3861–3876.

Arslan O and Koditschek DE (2017) Smooth extensions of feedback motion planners via reference governors. In: *IEEE International Conference on Robotics and Automation (ICRA)*.

Bhattacharya P and Gavrilova ML (2008) Roadmap-based path planning-using the voronoi diagram for a clearance-based shortest path. *IEEE Robotics & Automation Magazine* 15(2): 58–66.

- Borrmann U, Wang L, Ames AD and Egerstedt M (2015) Control barrier certificates for safe swarm behavior. *IFAC-PapersOnLine* : 68–73.
- Bravo JM, Alamo T and Camacho EF (2006) Robust mpc of constrained discrete-time nonlinear systems based on approximated reachable sets. *Automatica* 42(10): 1745–1751.
- De Luca A, Oriolo G and Samson C (1998) Feedback control of a nonholonomic car-like robot. In: *Robot motion planning and control*. Springer, pp. 171–253.
- Fisac JF, Chen M, Tomlin CJ and Sastry SS (2015) Reach-avoid problems with time-varying dynamics, targets and constraints. In: *International conference on hybrid systems: computation and control (HSCC)*. pp. 11–20.
- Fliess M, Lévine J, Martin P and Rouchon P (1995) Flatness and defect of non-linear systems: introductory theory and examples. *International Journal of Control (IJC)* 61(6): 1327–1361.
- Gao F, Wu W, Lin Y and Shen S (2018) Online safe trajectory generation for quadrotors using fast marching method and bernstein basis polynomial. In: *IEEE International Conference on Robotics and Automation (ICRA)*. pp. 344–351.
- Gao Y, Gray A, Tseng HE and Borrelli F (2014) A tube-based robust nonlinear predictive control approach to semiautonomous ground vehicles. *Vehicle System Dynamics* 52(6): 802–823.
- Garone E and Nicotra MM (2016) Explicit reference governor for constrained nonlinear systems. *IEEE Transactions on Automatic Control (TAC)* 61(5): 1379–1384.
- Harabor DD and Grastien A (2011) Online graph pruning for pathfinding on grid maps. In: *AAAI Conference on Artificial Intelligence*.
- Hart PE, Nilsson NJ and Raphael B (1968) A formal basis for the heuristic determination of minimum cost paths. *IEEE Transactions on Systems Science and Cybernetics* 4(2): 100–107.
- Herbert SL, Chen M, Han S, Bansal S, Fisac JF and Tomlin CJ (2017) FaSTrack: A modular framework for fast and guaranteed safe motion planning. In: *IEEE Conference on Decision and Control (CDC)*. pp. 1517–1522.
- İşleyen A, van de Wouw N and Arslan Ö (2022) Feedback motion prediction for safe unicycle robot navigation. *arXiv preprint arXiv:2209.12648*.
- Karaman S and Frazzoli E (2011) Sampling-based algorithms for optimal motion planning. *The International Journal of Robotics Research (IJRR)* 30(7): 846–894.
- Kavraki LE, Kolountzakis MN and Latombe JC (1998) Analysis of probabilistic roadmaps for path planning. *IEEE Transactions on robotics and automation (TRA)* 14(1): 166–171.
- Khalil H (2002) *Nonlinear systems*. Prentice Hall.
- Koenig S and Likhachev M (2006) Real-time adaptive A\*. In: *International Conference on Autonomous Agents and Multiagent Systems (AAMAS)*. ACM, pp. 281–288.
- Kohlbrecher S, Meyer J, von Stryk O and Klingauf U (2011) A flexible and scalable slam system with full 3d motion estimation. In: *IEEE International Symposium on Safety, Security and Rescue Robotics (SSRR)*. IEEE.
- Kousik S, Vaskov S, Bu F, Johnson-Roberson M and Vasudevan R (2020) Bridging the gap between safety and real-time performance in receding-horizon trajectory design for mobile robots. *The International Journal of Robotics Research (IJRR)* 39(12): 1419–1469.
- LaValle S (1998) Rapidly-exploring random trees: A new tool for path planning. Tr 98-11, Comp. Sci. Dept., Iowa State University.
- LaValle S (2006) *Planning Algorithms*. Cambridge University Press.
- Li Z, Arslan O and Atanasov N (2020) Fast and Safe Path-Following Control using a State-Dependent Directional Metric. In: *IEEE International Conference on Robotics and Automation (ICRA)*.
- Likhachev M, Gordon GJ and Thrun S (2004) ARA\*: Anytime A\* with provable bounds on sub-optimality. In: *Advances in neural information processing systems (NIPS)*. pp. 767–774.
- Liu S, Guo K, Yu X, Ma L, Xie L and Guo L (2023) Safe maneuvering planning for flights in complex environments. *IEEE Transactions on Industrial Electronics*.
- Liu S, Watterson M, Mohta K, Sun K, Bhattacharya S, Taylor CJ and Kumar V (2017) Planning dynamically feasible trajectories for quadrotors using safe flight corridors in 3-d complex environments. *IEEE Robotics and Automation Letters (RA-L)* 2(3).
- Nicotra MM and Garone E (2018) The explicit reference governor: A general framework for the closed-form control of constrained nonlinear systems. *IEEE Control Systems Magazine* 38(4): 89–107.
- Oleynikova H, Millane A, Taylor Z, Galceran E, Nieto J and Siegwart R (2016) Signed distance fields: A natural representation for both mapping and planning. In: *RSS 2016 Workshop: Geometry and Beyond-Representations, Physics, and Scene Understanding for Robotics*. University of Michigan.
- Pacelli V, Arslan O and Koditschek DE (2018) Integration of local geometry and metric information in sampling-based motion planning. In: *IEEE International Conference on Robotics and Automation (ICRA)*. pp. 3061–3068.
- Papachristodoulou A and Prajna S (2002) On the construction of Lyapunov functions using the sum of squares decomposition. In: *IEEE Conference on Decision and Control (CDC)*, volume 3. pp. 3482–3487.
- Perez A, Platt R, Konidaris G, Kaelbling L and Lozano-Perez T (2012) LQR-RRT\*: Optimal sampling-based motion

- planning with automatically derived extension heuristics. In: *IEEE International Conference on Robotics and Automation (ICRA)*. pp. 2537–2542.
- Quan L, Zhang Z, Zhong X, Xu C and Gao F (2021) Eva-planner: Environmental adaptive quadrotor planning. In: *2021 IEEE International Conference on Robotics and Automation (ICRA)*. IEEE, pp. 398–404.
- Santillo M and Jankovic M (2020) Collision Free Navigation with Interacting, Non-Communicating Obstacles. *arXiv preprint arXiv:2008.12092* .
- Squires E, Pierpaoli P and Egerstedt M (2018) Constructive barrier certificates with applications to fixed-wing aircraft collision avoidance. In: *IEEE Conference on Control Technology and Applications (CCTA)*. pp. 1656–1661.
- Webb DJ and van den Berg J (2013) Kinodynamic RRT\*: Asymptotically optimal motion planning for robots with linear dynamics. In: *IEEE International Conference on Robotics and Automation (ICRA)*.